Cell Reports
Article

Live-Cell Visualization of Pre-mRNA Splicing with Single-Molecule Sensitivity

Robert M. Martin,[1,3] José Rino,[1,3] Célia Carvalho,[1,3] Tomas Kirchhausen,[2,*] and Maria Carmo-Fonseca[1,*]
[1]Instituto de Medicina Molecular, Faculdade de Medicina, Universidade de Lisboa, 1649-028 Lisboa, Portugal
[2]Departments of Cell Biology and Pediatrics, Harvard Medical School and Program in Molecular and Cellular Medicine, Boston Children's Hospital, Boston, MA 02115, USA
[3]These authors contributed equally to this work
*Correspondence: kirchhausen@crystal.harvard.edu (T.K.), carmo.fonseca@fm.ul.pt (M.C.-F.)
http://dx.doi.org/10.1016/j.celrep.2013.08.013

SUMMARY

Removal of introns from pre-messenger RNAs (pre-mRNAs) via splicing provides a versatile means of genetic regulation that is often disrupted in human diseases. To decipher how splicing occurs in real time, we directly examined with single-molecule sensitivity the kinetics of intron excision from pre-mRNA in the nucleus of living human cells. By using two different RNA labeling methods, MS2 and λN, we show that β-globin introns are transcribed and excised in 20–30 s. Furthermore, we show that replacing the weak polypyrimidine (Py) tract in mouse immunoglobulin μ (IgM) pre-mRNA by a U-rich Py decreases the intron lifetime, thus providing direct evidence that splice-site strength influences splicing kinetics. We also found that RNA polymerase II transcribes at elongation rates ranging between 3 and 6 kb min^{-1} and that transcription can be rate limiting for splicing. These results have important implications for a mechanistic understanding of cotranscriptional splicing regulation in the live-cell context.

INTRODUCTION

In eukaryotes, extensive modification and alternative processing of the initial products of gene transcription can profoundly affect the diversity and function of the proteins that are generated from a single gene (Nilsen and Graveley, 2010). In addition to providing a versatile means of genetic regulation, removal of introns from pre-mRNAs by splicing is implicated in many human genetic diseases as either a direct cause, a modifier of disease severity, or a determinant of disease susceptibility (Cooper et al., 2009).

Splicing is carried out by the spliceosome, an elaborate macromolecular machine composed of uridine-rich small nuclear RNAs (UsnRNAs) packaged as ribonucleoprotein particles (snRNPs) that in human cells function in conjunction with over 200 distinct non-snRNP auxiliary proteins (Will and Lührmann, 2011). Spliceosomes build anew on every intron that is synthesized and then disassemble for the next round of splicing (Staley and Guthrie, 1998). Thus, unlike many other cellular enzymes that contain preformed, stable active sites, the spliceosome exhibits exceptional compositional and structural dynamics. In a recent study, the dynamic assembly of a single spliceosome was followed in real time in whole-cell extracts (Hoskins et al., 2011). That study revealed that association of spliceosomal subcomplexes with pre-mRNA occurs in an ordered pathway, that every subcomplex binding step is reversible, and that early binding events do not fully commit a pre-messenger RNA (pre-mRNA) to splicing (Hoskins et al., 2011). This implies that potentially any step during spliceosome formation might be subject to regulation. Spliceosome assembly is indeed highly regulated: depending on the combinatorial effect of proteins that either promote or repress the recognition of the core splicing sequences, splice sites in pre-mRNA can be differentially selected to produce multiple mRNA isoforms through alternative splicing.

In vitro, transcripts generated by RNA polymerase II are spliced within 15–60 min (Das et al., 2006). In contrast, electron microscopy analysis of *Drosophila* embryo genes and Balbiani ring genes in the salivary glands of the dipteran *Chironomus tentans* revealed that intron excision occurs within 2.5–3 min after transcription (Beyer and Osheim, 1988; Wetterberg et al., 2001), which suggests that pre-mRNA splicing is much more efficient in the cell nucleus than in nuclear extracts. Moreover, a large body of compelling evidence indicates that pre-mRNA splicing is tightly coupled to transcription and therefore should not be studied in isolation from other stages of gene expression (Maniatis and Reed, 2002). In particular, a kinetic model was proposed in which the spliceosome requires more time to assemble at certain regulated splice sites, and depending on the elongation rate, such sites can be recognized when transcription is slow, but skipped when transcription is fast (de la Mata et al., 2003; Eperon et al., 1988; Nogues et al., 2002). However, no study to date has directly compared the splicing kinetics of pre-mRNAs containing distinct splice sites.

Here, we monitored splicing and intron turnover by combining genomic integration of a single reporter gene in human cells,

intron labeling with fluorescent proteins, and spinning-disk confocal microscopy. We successfully measured the lifetime of single introns in the nucleus of living cells, and we show that different types of introns have distinct splicing kinetics depending on their size, splice-site strength, and relative position in the transcript.

RESULTS

Assay to Visualize Intron Removal from pre-mRNA in Living Cells

As a first model system, we used the well-characterized human β-globin (*HBB*) gene. The *HBB* gene has a simple structure composed of two constitutively spliced introns (Figure 1A), and the processes that lead to maturation of its primary transcripts have been extensively studied both in vitro and in vivo. In order to make β-globin pre-mRNA visible in living cells, we inserted binding sites for either the coat protein of bacteriophage MS2 or the antiterminator protein N of bacteriophage λ into each intron (Figures 1A and S1) and stably integrated the resulting transgenes into the genome of human host cells. Each MS2 binding site consists of a 19 nt RNA stem loop containing a single base change that significantly enhances MS2 coat protein binding (Lowary and Uhlenbeck, 1987), whereas λN binds to a minimal 15 nt RNA stem loop termed boxB (Franklin, 1985). A cassette coding for 24 tandemly repeated MS2 stem loops or 25 boxB repeats was inserted into either the first or second intron, preserving the consensus 5′ splice donor, lariat branch point, and 3′ splice acceptor sites. To avoid lack of control over the copy number and position of the integrated transgenes, we used a strategy that involves the site-specific recombinase Flp (flippase). Thus, all cell lines generated in this study have a single *HBB* gene integrated at the same site in the genome. Transcription of the *HBB* gene is driven by the human cytomegalovirus (CMV) promoter, and conditional expression of β-globin is regulated by a system derived from the tetracycline-resistance operon (TetO) (Figure 1A).

We engineered three isogenic human embryonic kidney 293 (HEK 293) cell lines that stably express a single copy of the *HBB* gene. The first cell line expresses a nontagged version of the *HBB* gene, so in order to have the two introns with approximately the same length, we used a *HBB* variant with a shorter intron 2 (β-WTΔ; Figure S1). The second cell line expresses the *HBB* gene tagged with λN binding sites in the first intron and MS2 binding sites in the second intron (β-λM; Figure S1). The third cell line expresses the *HBB* gene tagged with MS2 binding sites in the first intron and λN binding sites in the second intron (β-Mλ; Figure S1).

These cells were transiently transfected with plasmids encoding the GFP fused in-frame to either the carboxyl terminus of MS2 coat protein (MS2-GFP) or λN protein (λN-GFP). Both fusion proteins contain a nuclear localization signal that confines the chimera to the nucleus. When the GFP fusion proteins were expressed in the absence of transcriptional activation of the *HBB* gene by tetracycline, diffuse fluorescence was detected throughout the nucleus and tended to accumulate in nucleoli. Following transcriptional induction, a fluorescent dot was detected in the nucleoplasm (Figure 1B).

To determine whether the insertion of MS2 and λN binding sites in introns interfered with pre-mRNA splicing, we carried out RT-PCR analysis. RNA was isolated from cells expressing wild-type β-globin (i.e., devoid of MS2 or λN binding sites) and cells coexpressing the intronically tagged β-globin variants and MS2 and λN fusion proteins. RNA was reversed transcribed using an oligonucleotide that is complementary to a sequence downstream of the β-globin poly(A) site. The resulting complementary DNA (cDNA) was then PCR amplified using primers that specifically detect spliced and unspliced β-globin transcripts (Figure 1C; Table S1). This RT-PCR experiment detects transcripts that have not yet been cleaved at the poly(A) site and therefore are expected to be close to the gene template. The results indicate that β-globin pre-mRNA molecules tagged with intronic MS2 and λN fluorescent fusion proteins are already spliced while the transcripts are still uncleaved. However, compared with wild-type pre-mRNAs, transcripts containing tagged introns are less efficiently spliced. This implies that tagged pre-mRNAs take longer to be spliced and/or that some may fail to be spliced.

We next examined the localization of RNAs tagged with MS2 stem loops by fluorescent in situ hybridization (FISH). Cells expressing β-λM transcripts were hybridized with a probe complementary to the MS2 stem loops and a probe complementary to the hygromycin resistance gene in the plasmid used for transfection, which reveals the site of integration of the *HBB* gene in the host genome (Figure 1D). The resulting nuclear dots colocalized, showing that intronic MS2 stem loops are predominantly detected at the transcription site. Cells were alternatively hybridized with a probe complementary to the MS2 stem loops and a probe complementary to full-length β-globin RNA (Figure S2). We observed precise colocalization of fluorescent dots, indicating that the majority of intronic MS2 stem loops detected in the nucleus are either part of nascent pre-mRNA molecules or correspond to excised introns located in close proximity to the transcription site. The observation that introns appear to be restricted to the transcription site is consistent with our previous data indicating that β-globin pre-mRNA is spliced cotranscriptionally (Custódio et al., 1999; de Almeida et al., 2010). Moreover, we have shown that splicing-defective mutant β-globin pre-mRNAs are retained at the transcription site (Custódio et al., 1999; de Almeida et al., 2010). A similar retention mechanism could explain why we do not detect unspliced tagged RNAs in the nucleoplasm.

Monitoring the Dynamics of Intron Turnover at the Transcription Site

Time-lapse, multiplane, spinning-disk confocal microscopy was used to monitor intron dynamics at the site of transcription. An immediate observation in the recorded movies was that the fluorescence intensity was not constant over time, but rather showed cycles of fluorescence gain and loss (Movie S1). If the observed increase in fluorescent signal results from binding of MS2- or λN-GFP fusion proteins to newly synthesized MS2 or λN stem loops, the appearance of a fluorescent dot will require

Cell PRESS
Open ACCESS

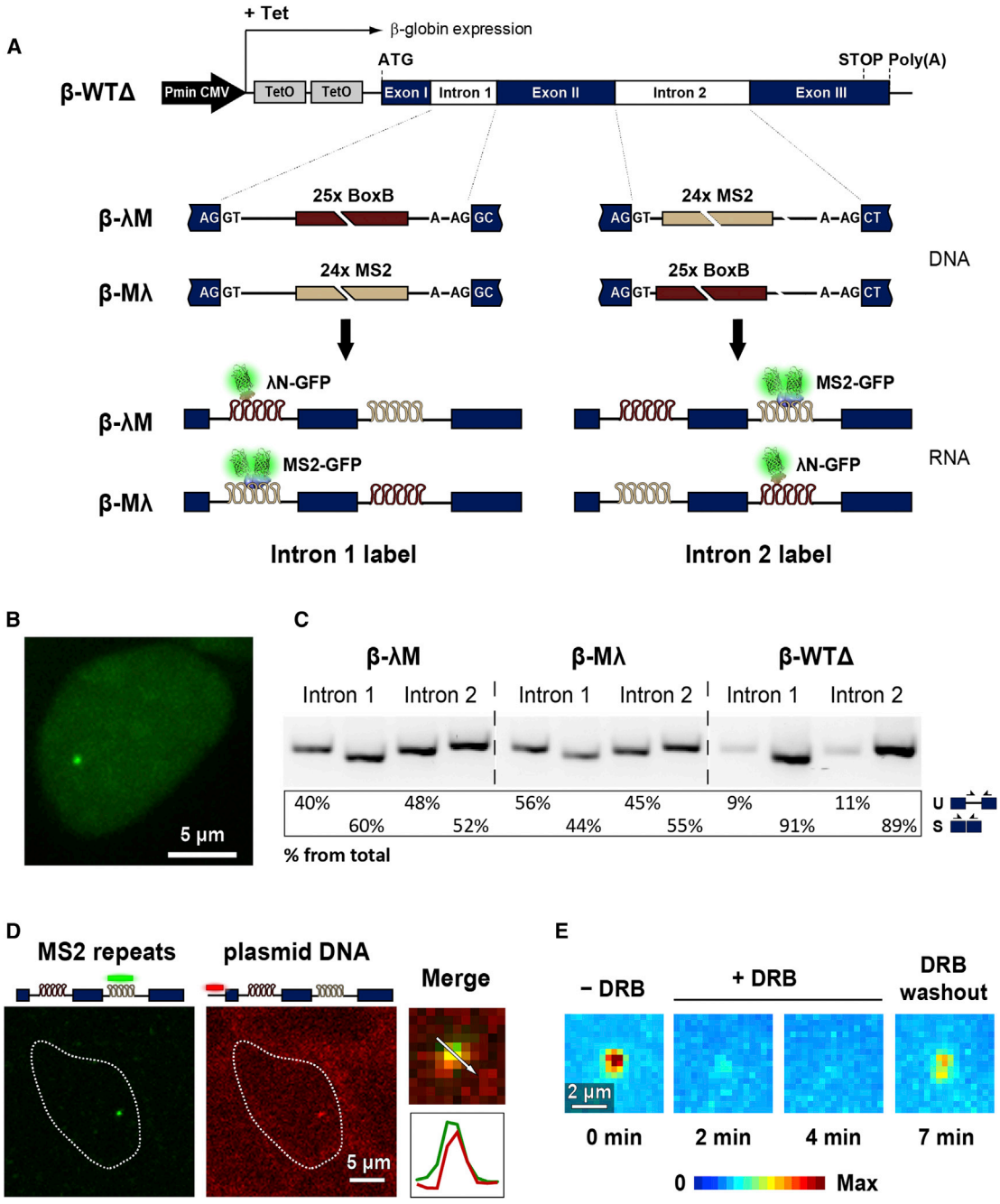

Figure 1. Visualization of β-Globin Introns

(A) Illustration of the structure of the *HBB* transgene. Tetracycline-inducible expression is under the control of a minimal human CMV promoter (Pmin CMV). Binding sites for MS2 and λN were inserted into either the first or second intron. The interaction of MS2 and λN proteins fused to GFP with the intronic stem loops allows the transcribed pre-mRNAs to be visualized.

(B) Representative HEK293 cell expressing β-globin transcripts tagged with MS2-binding sites in the second intron. Cells were transiently transfected with a plasmid encoding MS2-GFP and imaged after incubation with tetracycline.

(C) RT-PCR analysis of β-globin RNA uncleaved at the poly(A) site. RNA was extracted from cells that express the β-globin transcripts tagged in the first or second intron with MS2 and λN fluorescent fusion proteins. PCR primers (arrows) used to detect spliced (S) and unspliced (U) RNA, and results from semiquantitative analysis of PCR product abundance are shown in the diagram.

(D) Double RNA and DNA FISH shows introns labeled with MS2 at the transcription site. After transcriptional induction, cells expressing β-λM transcripts were fixed and hybridized with Cy5-labeled probe complementary to the MS2 repeats (RNA FISH, pseudocolored green) and Cy3-labeled probe targeting the vector used for β-globin gene integration (DNA FISH, pseudocolored red). Double-hybridization merged images are shown and enlarged insets depict the transcription site with the corresponding intensity line scans.

(legend continued on next page)

ongoing transcription. We therefore treated cells coexpressing β-λM transcripts and MS2-GFP with the reversible inhibitor of transcription 5,6-dichloro-1-β-D-ribobenzimidazole (DRB). Figure 1E shows maximum-intensity z-projection images of the β-globin transcription site in a cell before and after treatment with DRB. After the DRB was washed out, the same cell was reimaged, revealing the reappearance of the fluorescent signal (Figure 1E). Time-lapse analysis of 30 cells indicated that the fluorescence intensity at the transcription site decreased progressively, and the signal was no longer distinguishable from background fluorescence after incubation with DRB for 4–5 min. The signal consistently reappeared within 2–3 min after the DRB was washed out. These results support the view that the fluorescent signal at the transcription site results from synthesis of RNA sequences that bind GFP fusion proteins. Because the arrays of RNA motifs that bind MS2 and λN proteins form stem-loop structures, it is estimated that they occupy a volume of <250 nm in diameter (assuming a length of 0.3 nm/nt; see also Grünwald and Singer, 2010). Thus, they should appear as diffraction-limited objects.

In order to rigorously quantify the fluorescence emitted from a single transcription site, we developed an image analysis application (Figure S3) to track single transcription sites in three dimensions and quantify their total fluorescence intensity (TFI) over time by Gaussian fitting (Figures 2A–2C). As graphically depicted in Figure 2D, the fluorescence intensity shows fluctuations with time, with TFI increasing to a given maximum and returning to background levels. Similar results were observed for the first and second β-globin introns labeled with either MS2 or λN-GFP fusion proteins (Figure S4).

Assuming that increments in the fluorescence signal result from de novo transcription of intronic MS2 or λN-binding sites, fluorescence loss could reflect either intron excision or release of unspliced RNA from the site of transcription. Although we cannot rule out the possibility that some unspliced RNAs are released to the nucleoplasm, the observation that approximately 50% of fluorescently tagged β-globin introns are spliced before cleavage at the poly(A) site (Figure 1C) argues that at least half of the fluorescence-loss events are due to splicing.

The First and Second β-Globin Introns Have Different Lifetimes

Fluctuations in TFI values measured at the transcription site were visible in most time-lapse series, with significant cell-to-cell variation in the patterns of fluorescence gain and loss. Although in some time-lapse series the TFI did not drop to background levels, in many movies the phase of fluorescence loss reached background level (Figure 2D). In light of the recent finding that in mammalian cells pre-mRNAs are synthesized in bursts (Chubb and Liverpool, 2010), we consider it most likely that a complete disappearance of fluorescence reflects a period of transcriptional silence during which introns are excised from all previously synthesized pre-mRNAs. An analysis of time-lapse series with fluctuations around background reveals two types of cycles. The first is generally longer than 200 s, reaches high fluorescence intensity values, and shows a complex pattern of subfluctuations. The second is much shorter (typically <50 s) and has lower fluorescence intensity values (Figure 2D). Since high fluorescence intensity indicates accumulation of multiple transcripts, we sought to estimate how many pre-mRNA molecules were present at the transcription site during each cycle of fluorescence gain and loss. For this purpose, we took advantage of spliceostatin A (SSA), a potent splicing inhibitor that induces leakage of unspliced β-globin pre-mRNAs to the nucleoplasm (Martins et al., 2011). SSA inhibits splicing in vivo and in vitro by targeting the SF3b complex and blocking the formation of a catalytic spliceosome subsequent to the recruitment of U2 snRNP to the pre-mRNA (Corrionero et al., 2011; Kaida et al., 2007; Roybal and Jurica, 2010). Live-cell imaging of cells treated with 100 ng ml^{-1} SSA for 4–8 hr revealed a multitude of diffraction-limited objects diffusing throughout the nucleus, and similar results were observed for introns labeled with either MS2 or λN-GFP fusion proteins (Figures 3A and 3C; Movie S2). Based on previous studies (Grünwald and Singer, 2010; Larson et al., 2011; Shav-Tal et al., 2004), we reasoned that the diffraction-limited objects that diffuse throughout the nucleus of SSA-treated cells correspond to individual mRNP particles, each containing a single fluorescently labeled intron. In agreement with this view, images of diffusing introns labeled with either MS2 or λN-GFP show single-peaked distributions of fluorescence intensity values (Figures 3B and 3D), indicating that the population of unspliced RNA primarily consists of individual particles. These observations further demonstrate that if unspliced pre-mRNAs were diffusing away from the transcription site in untreated cells, they would be detected by our visualization system.

In parallel, we determined the TFI emitted by a single GFP molecule. For this, we used either purified single GFP molecules (Figure 3E) or particles containing three GFP molecules synthesized in tandem (Figure 3H). Single and triple GFP molecules were adsorbed to the surface of glass coverslips and imaged as isolated diffraction-limited fluorescent objects. Bleaching of GFP molecules was induced by continuous imaging while fluorescence intensity was monitored as a function of time (Figures 3E and 3H). Bleaching of single GFP molecules occurred in a single step (Figure 3F), whereas up to three photobleaching events were detected for the triple GFP particles (Figure 3I), as expected assuming that each GFP molecule in the triple particle undergoes independent stochastic bleaching. The distribution of ΔTFI estimated for single GFP bleaching events is depicted in Figure 3G. The results show that the average ΔTFI associated with bleaching events on single GFP molecules is similar to the most observed average ΔTFI corresponding to single bleaching steps in triple GFP particles (Figure 3J). We used the average

(E) A spinning-disk confocal microscope was used to obtain 4D movies of cells expressing β-globin transcripts tagged with MS2-GFP in the second intron, and z stacks of optical sections were obtained every 60 s. Maximum-intensity projection images of fluorescence at the transcription site were generated for each time point and pseudocolored. Images were acquired before (−DRB) and after (+DRB) incubation with 75 μM DRB for 2 and 4 min. The DRB was subsequently washed out and 7 min later the same transcription site was reimaged.
See also Figures S1, S2, and Table S1.

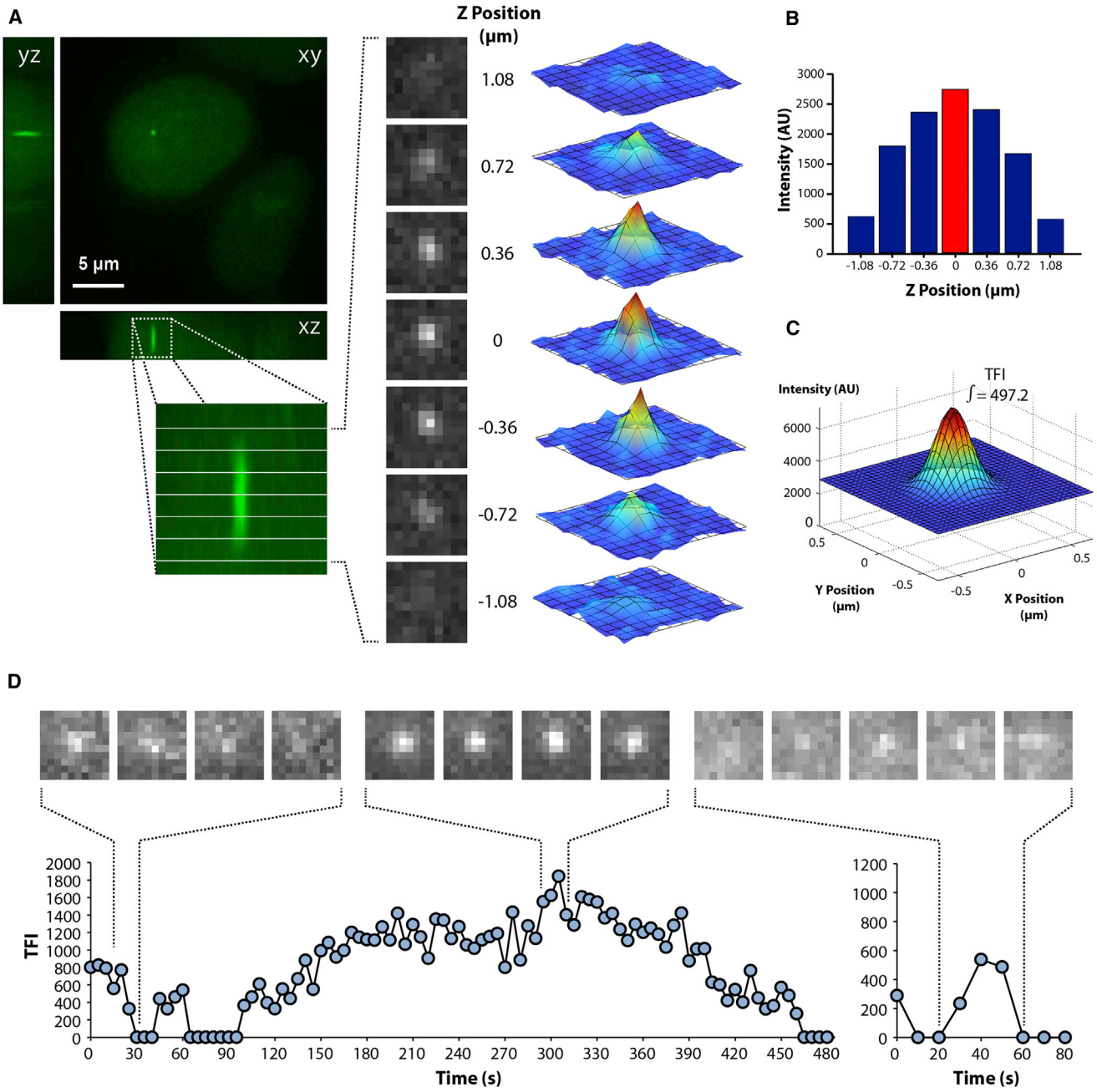

Figure 2. Fluctuations in Fluorescence Intensity at the Transcription Site

For quantification of TFI, a z stack of eight optical sections spaced by 0.36 µm and centered on the transcription site was recorded at 5 s intervals.

(A) The diffraction-limited fluorescent dot is visible in the central planes of the z stack as a rotationally symmetric point spread function that is longer along the optical z axis, as expected. Each of the images in these central planes can be fitted by a 2D Gaussian function.

(B) At each time point, we tracked the position of the transcription site in 3D and determined the plane corresponding to the highest intensity value.

(C) A 2D Gaussian fit was performed at the plane of highest intensity and the result was plotted as an analytical 2D Gaussian function, the integral of which was defined as the TFI for the transcription site.

(D) For each time-lapse series, the TFI was plotted over time in line graphs. A sequence of images depicting fluorescence fluctuations in the highest-intensity plane is shown on top of each graph.

See also Figure S3 and Movie S1.

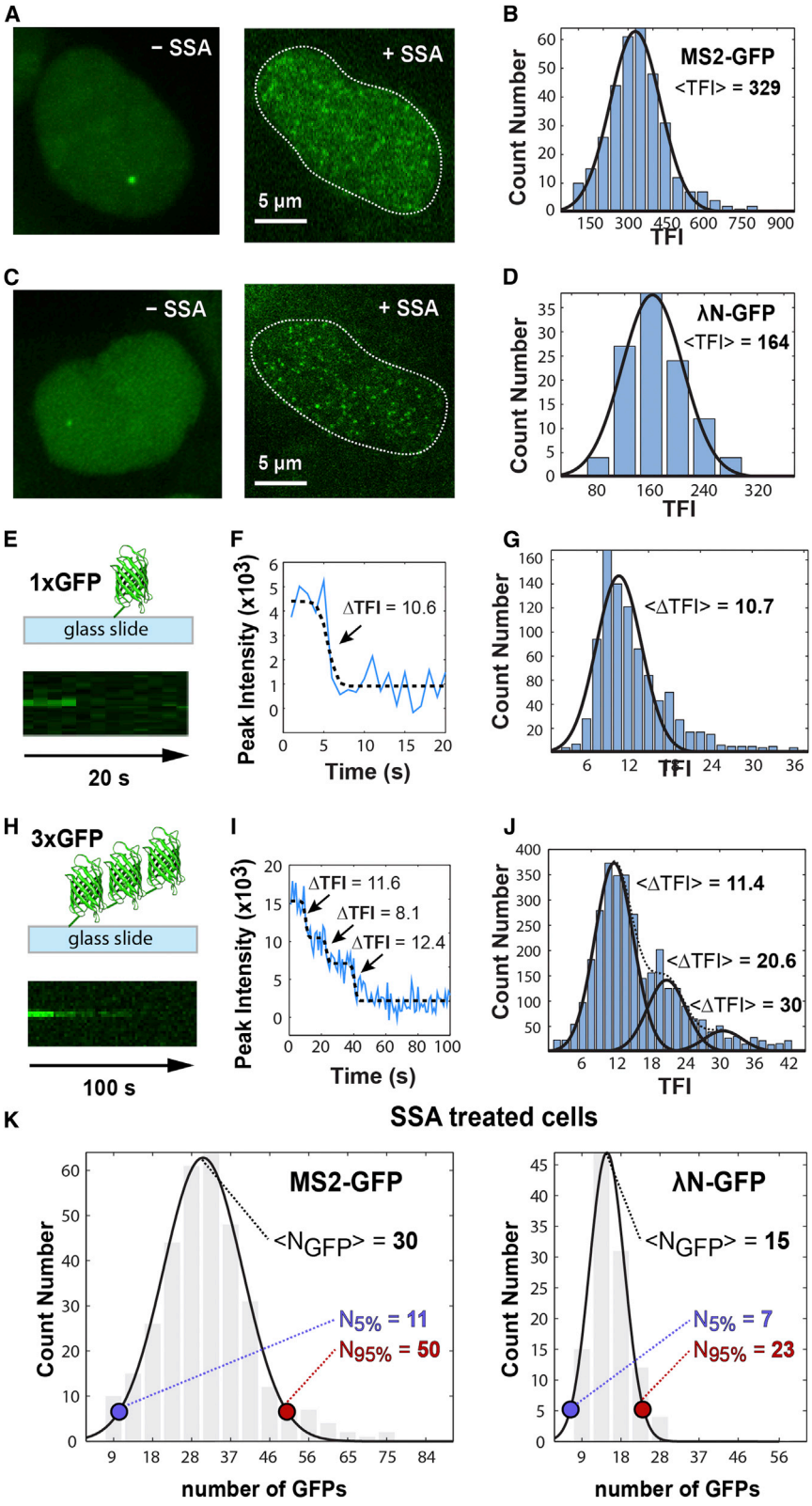

Figure 3. Counting the Number of Introns at the Transcription Site

(A and C) Single optical plane images of cells expressing β-λM transcripts tagged with MS2-GFP (A) and λN-GFP (C) were imaged before and after treatment with 100 ng ml^{-1} SSA for 4–8 hr. In contrast to transcription sites that are relatively immobile in the nucleus, unspliced introns in SSA-treated cells diffuse rapidly throughout the nucleoplasm (Movie S2).

(B and D) Distributions of TFI measured in SSA-treated cells expressing β-λM transcripts tagged with MS2-GFP (B) and λN-GFP (D). TFI was estimated by 2D Gaussian fitting as described in Figure 2.

(E and H) Schematic illustrating GFP molecules adsorbed to glass coverslips (top) and a pseudo-line plot (xt plot obtained from the xyt time course) of the photobleaching sequence (bottom). We analyzed single GFP molecules (E) and particles containing three GFP molecules synthesized in tandem (H). A single optical plane was continuously recorded using 1 s exposure per image.

(F and I) The intensity profile over time was plotted in a graph and fitted to a sigmoid-shaped function for single GFP molecules (black dashed line in F) or the sum of sigmoid-shaped functions for triple GFP particles (black dashed line in I) to detect bleaching events. The ΔTFI associated with each bleaching event was estimated by 2D Gaussian fitting and normalized for an exposure time of 15 ms for direct comparison purposes (see Experimental Procedures). Arrows indicate photobleaching of one GFP molecule.

(G) Distribution of ΔTFI corresponding to bleaching events for single GFP molecules (n = 1,001). Data from a total of 420 images were recorded in 22 time series.

(J) Distribution of ΔTFI corresponding to bleaching events for triple GFP particles (n = 3,358). The first peak corresponds to single bleaching events, the second peak corresponds to two simultaneous bleaching events, and the third peak is due to the less frequent situation of bleaching of three GFP molecules at the same time point. Data from a total of 931 images were recorded in 22 time series.

(K) Distribution of GFP molecules bound to individual unspliced pre-mRNA molecules diffusely detected in the nucleoplasm of SSA-treated cells. Data from the histograms depicted in (B) and (D) were calibrated using 10.7 as the average TFI corresponding to a single GFP molecule (for 15 ms exposure time). $N_{5\%}$ and $N_{95\%}$ indicate the lower and upper limits, respectively, for the number of GFPs contained within 2 SDs of the average value (~95% of values).

See also Movie S2.

ΔTFI corresponding to the amount of light emitted by a single GFP molecule to calibrate the TFI measurements of single introns obtained from SSA-treated cells. The results show that on average, each MS2-labeled intron binds 30 GFPs and each λN-labeled intron binds 15 GFPs, with distributions ranging between 11 and 50 (for 2 SDs: 95%) for MS2 and between 7 and 23 (95%) for λN (Figure 3K). This is in very good agreement with the maximum number of GFP molecules expected to bind to a single intron labeled with 24 MS2 stem loops or 25 boxB motifs, taking into account that the MS2 protein binds as a dimer (Valegård et al., 1994) and that the boxB detection system we used is composed of four copies of λN peptide fused to three monomeric GFP molecules (Daigle and Ellenberg, 2007). Thus, our quantitative data are consistent with the view that each particle diffusing in the nucleus of SSA-treated cells contains a single fluorescently labeled intron.

Having determined the TFI value that corresponds to a single fluorescently labeled intron, we next analyzed cycles of fluorescence gain and loss that started and returned to background level, and calculated the number of introns present when the TFI reached a maximum. We estimated that the long cycles involve the synthesis of more than five labeled introns, whereas the short cycles contain only one, two, or three introns (Figure 4A). This suggests that the long cycles result from transcriptional bursts that involve initiation by several consecutive polymerases, leading to superposition of multiple pre-mRNAs at distinct stages of their life cycle. Consistent with this view, during a long cycle we typically observe subfluctuations in intensity corresponding to the synthesis and disappearance of one or more introns. Such fluctuations are not observed in the short cycles. We therefore conclude that the long fluorescence cycles correspond to the time it takes to transcribe and process an asynchronous population of multiple pre-mRNAs. In contrast, the short cycles reflect the time it takes to transcribe and excise either a single intron or a group of two to three synchronous introns. Thus, the duration of a short cycle corresponds to the intron lifetime. We measured the duration of the short cycles and found that the most frequent lifetime value was 20 s for the first intron and 30 s for the second intron (Figures 4B and 4C). Similar lifetime distributions were observed for introns labeled with either MS2-GFP or λN-GFP (Figure S4), indicating that the observed intron kinetics is independent of the fluorescent labeling technique. These results also argue that the phase of fluorescence loss in the short cycles reflects splicing rather than release of unspliced RNAs from the site of transcription. Indeed, if transcripts were released unspliced, loss of fluorescence for pre-mRNAs labeled on the first intron would only occur after transcription elongation through the second intron and last exon (~2,000 nt). Thus, if transcripts were released unspliced, cycles of fluorescence gain and loss for the first intron should be longer than second-intron cycles.

To further confirm that loss of fluorescence is due to splicing and not to release of unspliced pre-mRNA, we sought to directly visualize the dynamics of both β-globin introns simultaneously. We reasoned that if transcripts were released unspliced, then fluorescence associated with the first intron should increase before fluorescence associated with the second intron, and both fluorescent signals should decrease simultaneously. Cells expressing the *HBB* gene tagged with λN binding sites in the first intron and MS2 binding sites in the second intron (β-λM) were cotransfected with two plasmids: one that encodes λN protein fused to GFP and one that encodes MS2 protein fused to the red fluorescent protein mCherry (Figure 4D). We captured three-dimensional (3D) time series at 5 s intervals following sequential illumination of the sample with the appropriate lasers, and calculated the TFI values. We observed that the green fluorescence intensity associated with intron 1 started to increase before the red fluorescence in intron 2, and then decreased while intron 2 red fluorescence was still increasing or at its maximum (Figure 4E). Similar results were observed in cells expressing the β-Mλ construct, with intron 1 labeled red and intron 2 labeled green (Figure 4F). These data strongly suggest that intron 1 is excised while intron 2 is still present in the nascent transcript, arguing against release of unspliced transcripts.

The Intron Lifetime Differs Depending on Splice-Site Strength and Intron Size

To study the effect of splice-site strength and intron size on the splicing kinetics, we introduced 24 tandemly repeated MS2 binding sites in mouse immunoglobulin μ (IgM) gene reporters (Figure 5A). A single copy of each transgene was stably integrated into the genome of HEK 293 cells through site-specific DNA recombination. In contrast to β-globin pre-mRNA, which contains strong splice sites and is constitutively spliced, mouse IgM is a regulated splicing substrate (Tsurushita et al., 1987; Watakabe et al., 1989). In particular, the intron between exons M1 and M2 contains weak 3′ splice-site sequences and requires an enhancer located in exon M2 for efficient splicing (Watakabe et al., 1993). To determine whether the presence of a weak or strong 3′ splice site affects the splicing kinetics, we compared wild-type IgM M1-M2 (IgM-weakPy; Figure 5A) and a mutant constructed by replacing the weak 12 nt polypyrimidine (Py) tract of IgM with the U-rich 14 nt Py tract of adenovirus major late promoter pre-mRNA (IgM-strongPy; Figure 5A). To investigate the influence of intron size on splicing kinetics, we extended the intron length in the IgM-strong Py construct by inserting fragments derived from the first intron of the mouse RNA polymerase II gene before and after the MS2 binding sites (Figures 5A and S5A).

Following transcriptional activation of the IgM reporter genes by tetracycline in cells expressing MS2-GFP, a fluorescent dot was detected in the nucleoplasm corresponding to nascent pre-mRNA (Figure 5B). Because the IgM reporter genes were engineered to encode a cyan fluorescent protein (CFP) fused to a peroxisomal targeting signal (PTS) at the carboxyl terminus, and the CFP-PTS sequence was inserted in frame with spliced M1 and M2 exons, detection of cyan fluorescence in peroxisomes confirmed that the pre-mRNAs were correctly spliced and exported to the cytoplasm (Figure S5B).

As previously described for β-globin RNA, we carried out an RT-PCR analysis of IgM RNA using for reverse transcription an oligonucleotide that is complementary to the sequence downstream of the poly(A) site (Figure 5C; Table S1). This analysis detects uncleaved RNAs, which are presumably still attached to the gene template at the site of transcription. Consistent with the finding that CFP is correctly targeted to peroxisomes, the RT-PCR results confirmed that all types of the tested pre-mRNAs

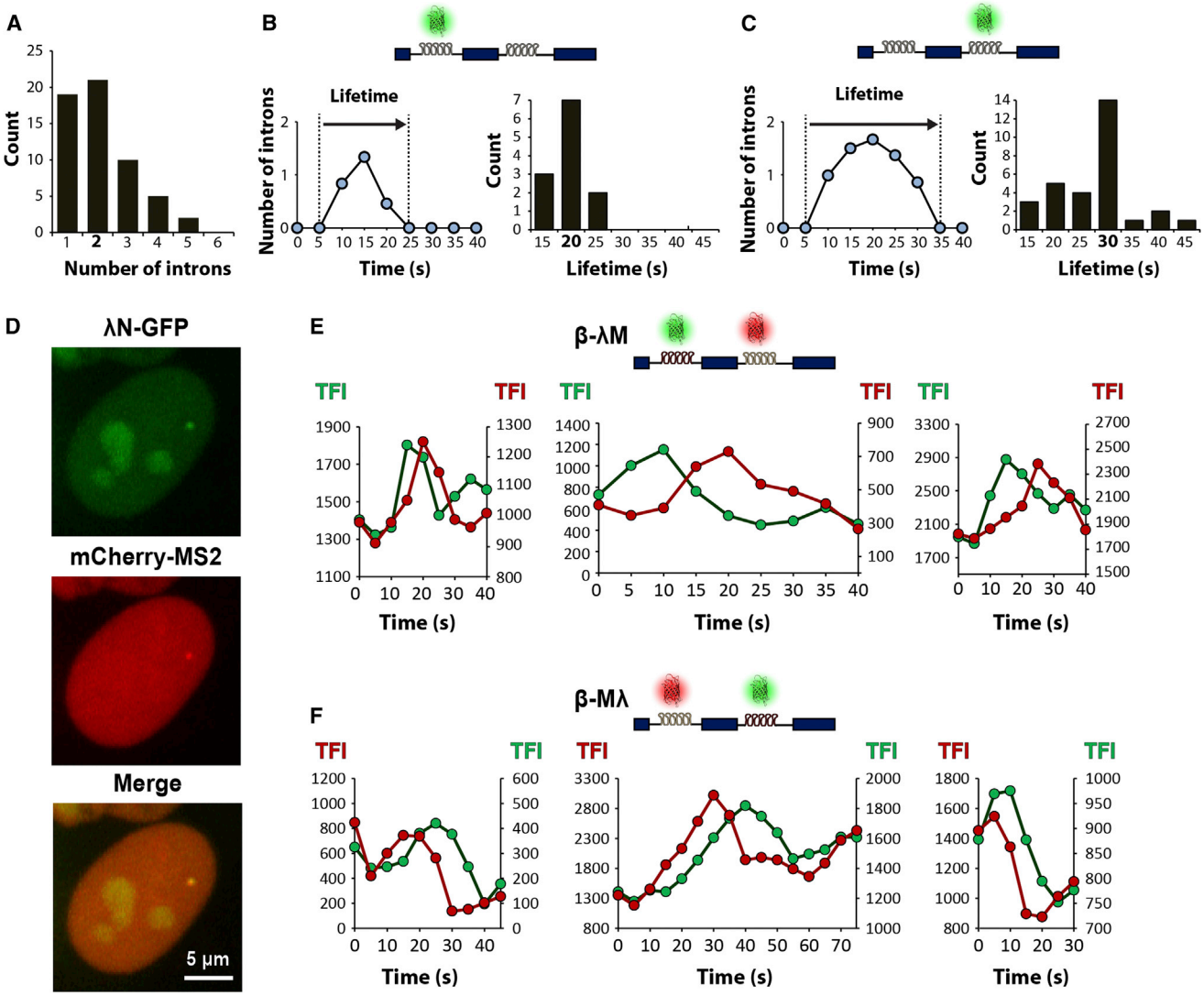

Figure 4. The First and Second β-Globin Introns Have Distinct Lifetimes

(A) Distribution of the number of introns present at the transcription site when the TFI reaches maximum value, for short cycles starting and returning to background fluorescence. Data from 57 cycles observed in 41 independent time-lapse sequences of cells expressing λN-GFP or MS2-GFP labeling either the first or second intron.

(B) Representative graph depicting a cycle of fluorescence gain and loss in a cell expressing β-globin transcripts tagged in the first intron. TFI was converted into number of introns. The lifetime is defined as the total duration of the cycle. The histogram on the right depicts the distribution of lifetime values (n = 38).

(C) Representative graph depicting a cycle of fluorescence gain and loss in a cell expressing β-globin transcripts tagged in the second intron. The histogram on the right depicts the distribution of lifetime values (n = 75).

(D) Simultaneous detection of both β-globin introns: representative maximum-intensity projection image of a cell expressing the *HBB* gene tagged with λN binding sites in the first intron and MS2 binding sites in the second intron (β-λM cell line), and cotransfected with λN-GFP (green) and mCherry-MS2 (red).

(E) Dual-line plots of TFI over time for cycles observed in β-λM cells, with first intron labeled with λN-GFP (green) and second intron labeled with mCherry-MS2 (red).

(F) Dual-line plots of TFI over time for cycles observed in β-Mλ cells, with the first intron labeled with mCherry-MS2 (red) and the second intron labeled with λN-GFP (green).

See also Figure S4.

were spliced. However, the proportion of spliced relative to unspliced RNA differed between constructs, being highest (>90%) for IgM+1700 (Figure 5C). Compared with the other constructs, the MS2 array of IgM+1700 is farther away from both the 5′ and 3′ splice sites. This may reduce interference with spliceosome assembly, thereby resulting in higher splicing efficiency.

Fluctuations in fluorescence intensity at the site of transcription were quantitatively analyzed as described above for β-globin pre-mRNA. To estimate the intron lifetimes, we selected

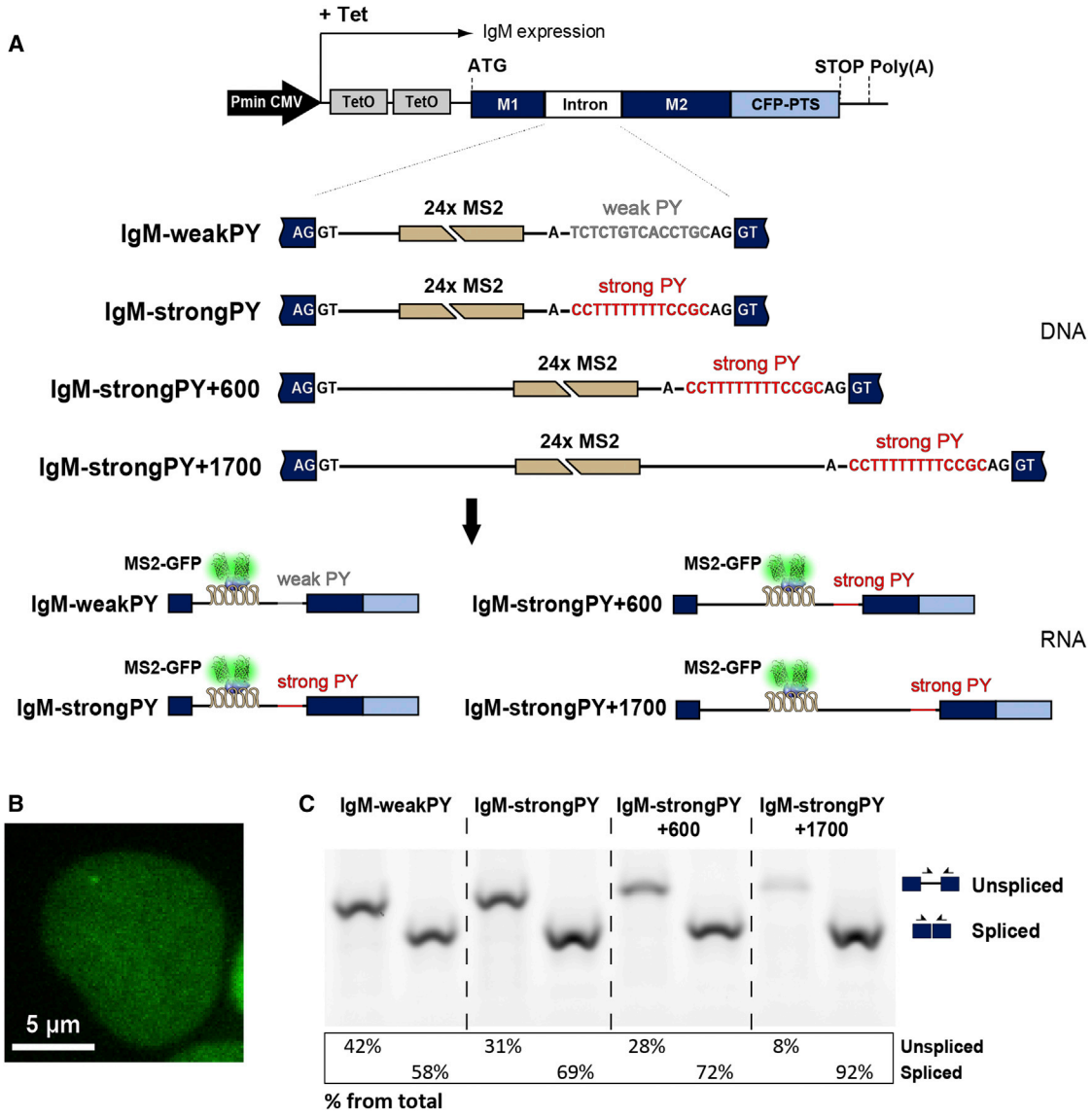

Figure 5. Visualization of the Intron Located between IgM Exons M1 and M2

(A) Illustration of the structure of the IgM transgenes. Tetracycline-inducible expression is under the control of a minimal human CMV promoter (Pmin CMV). Binding sites for MS2 were inserted as indicated. The interaction of MS2-GFP with the intronic stem loops allows the transcribed pre-mRNAs to be visualized.

(B) Representative HEK 293 cell expressing IgM-weakPy transcripts. Cells were transiently transfected with a plasmid encoding MS2-GFP and imaged after incubation with tetracycline.

(C) RT-PCR analysis of IgM RNA uncleaved at the poly(A) site. RNA was extracted from the indicated cell lines. PCR primers (arrows) used to detect spliced and unspliced RNA, and results from semiquantitative analysis of PCR product abundance are shown in the diagram.

See also Figure S5 and Table S1.

discrete cycles of fluorescence starting at background level and involving synthesis of a single transcript (Figures 6A and S6). The results show that IgM introns with weak Py tract have an average lifetime of 43 ± 14 s (n = 31). In contrast, introns with strong Py tract have a significantly shorter lifetime: 31 ± 6 s (n = 37; p = 4.3 × 10^{-6}). As expected, compared with the short IgM pre-mRNA with a strong Py tract, inserting ~600 nt upstream of the MS2 array does not significantly affect the duration of the discrete cycles of fluorescence (31 ± 8 s; n = 29). These cycles no longer correspond to the full intron lifetime because the time it takes to synthesize the extra 600 nt before the MS2 array is not detected. Insertion of ~1,000 nt downstream of the MS2 array, on the contrary, results in significantly longer cycles of fluorescence (49 ± 14 s; n = 33; p = 9.6 × 10^{-9}; Figures 6B and 6C).

We also determined the time elapsed since the fluorescence intensity starts to increase above background until it peaks (Figure 6D) and we obtained the distribution shown in Figure 6E. From this, we conclude that RNA polymerase II transcribes the

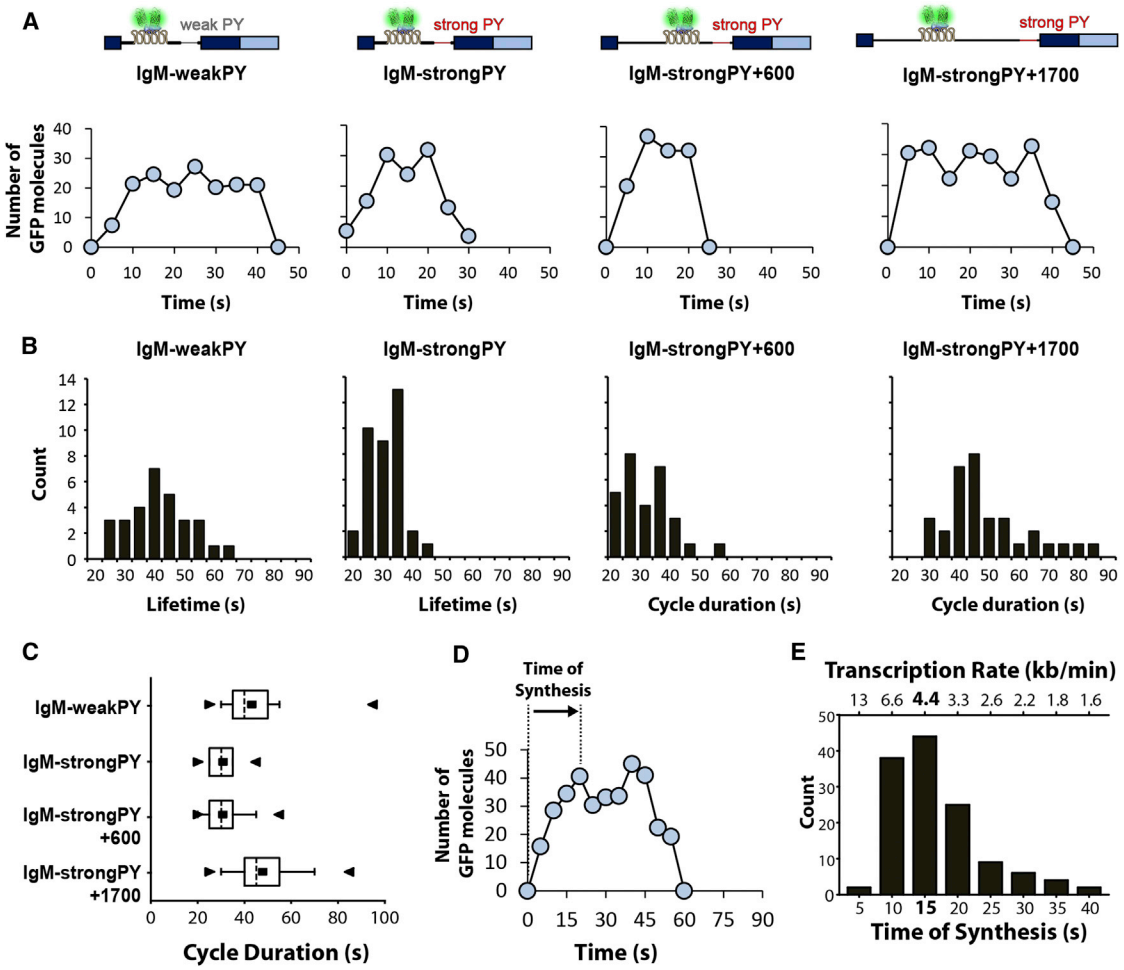

Figure 6. Intron Lifetime Is Influenced by Splice-Site Strength and Intron Size

(A) Representative graphs depicting cycles of fluorescence gain and loss involving synthesis of a single transcript (maximum fluorescence intensity up to 40 GFP molecules) in cells expressing the indicated IgM constructs. TFI was converted into number of GFP molecules.

(B) Histograms showing the duration of cycles of fluorescence gain and loss involving synthesis of a single transcript. In the case of IgM-weakPY and IgM-strongPY constructs, the cycle duration values correspond to intron lifetime; for IgM-strongPy+600 and IgM-strongPY+1700 constructs, the cycle duration excludes time of synthesis of the ~600 nt transcribed before the MS2 array.

(C) Box-and-whisker plots of lifetime values for the indicated IgM constructs showing the mean (■), median (dotted line), minimum (▶), maximum (◀), 25% quartile (box), and 10% quartile (whiskers).

(D) Representative graph depicting a cycle of fluorescence gain and loss involving synthesis of a single transcript. The time of synthesis of the MS2 array (1,093 nt) is defined as the time elapsed since fluorescence intensity starts to increase above background until it reaches a maximum level.

(E) Distribution of the values estimated for time of synthesis and rates of transcription (n = 130).

See also Figure S6.

array of MS2 stem loops (~1,093 nt) at rates ranging predominantly between 3 and 6 kb min^{-1}. Assuming such elongation rates, transcription of the additional 1,000 nt present in the IgM+1700 intron would take 12–24 s. Thus, the prolonged fluorescent cycles observed for this construct most likely result from the extra time needed to transcribe the longer intron.

DISCUSSION

We have developed a system that makes it experimentally possible to observe in real time the transcription and turnover of fluorescently labeled introns in living cells with single-molecule resolution.

By using two different RNA labeling methods, MS2 and λN, we show that transcription and excision of β-globin introns occurs in 20–30 s, and that compared with the second intron, the first intron has a shorter lifetime. The longer lifetime of the second intron may relate to the fact that intron 2 in β-globin pre-mRNA is a terminal intron, and there is a well-established connection between splicing of terminal introns and 3′ end processing (Niwa et al., 1992). More specifically, cotranscriptional coupling between splicing of the β-globin last intron, 3′ end processing,

and transcriptional termination has been proposed to allow for a time lag that is important for a check on the integrity of the transcript before cleavage and release to the nucleoplasm (Dye and Proudfoot, 1999).

In addition to β-globin, we further engineered mouse IgM gene reporters containing a single intron between exons M1 and M2. When the weak wild-type Py tract was replaced by the strong Py of adenovirus major late promoter pre-mRNA, we observed a mean intron lifetime of 31 s. A significantly longer mean intron lifetime (43 s) was measured for the wild-type pre-mRNAs containing the weak Py tract, providing direct evidence that splice-site strength influences splicing kinetics.

We found that RNA polymerase II elongates through the DNA sequence corresponding to 24 MS2 binding sites inserted into an intron at rates between 3 and 6 kb min^{-1}. This is consistent with the previously reported value of 3.8 kb min^{-1} estimated by quantitative RT-PCR after reversible transcriptional inhibition induced by DRB (Singh and Padgett, 2009). An elongation rate of 4.3 kb min^{-1} was also inferred from computational models of photobleaching data obtained in living cells using a cassette coding for 24 binding sites for MS2 (Darzacq et al., 2007). In contrast, more recent real-time observations in yeast revealed slower transcription rates in the range of 1.2–2.7 kb min^{-1} (Hocine et al., 2013; Larson et al., 2011). In a study using global run-on sequencing, elongation rates were reported to vary as much as 4-fold (ranging between 0.37 and 3.57 kb/min) at different genomic loci and in response to different stimuli (Danko et al., 2013).

When we compared the duration of fluorescence cycles for short and long pre-mRNAs with a strong Py tract, we obtained mean values of 31 and 48 s, respectively. Based on the estimated elongation rates, we conclude that the extra time required to transcribe the longer intron is sufficient to account for the observed difference. Thus, our results indicate that transcription can be rate limiting for splicing. This finding may explain the slow splicing rates, ranging between 5 and 12 min, that have been reported for endogenous long mammalian genes (Kessler et al., 1993; Singh and Padgett, 2009). It is important to note, however, that splicing may not always occur immediately after transcription of the splice sites. Particularly in the case of alternative splicing, intron excision must be delayed until all sequences involved in the choice are transcribed. Accordingly, some regulated introns have been shown to be excised after release from the transcription site (Vargas et al., 2011), and a more recent global study suggests that a subset of splicing events are completed only after the polymerase transcribes past the poly(A) site, but before the mRNA is released (Bhatt et al., 2012).

In summary, our work provides a valuable experimental system that has already proved useful for addressing fundamental questions concerning the dynamic control of pre-mRNA splicing in living cells. We anticipate that improved methodologies for single and double labeling of individual pre-mRNA molecules (Wu et al., 2012), and in particular the ability to image endogenous RNA (Lionnet et al., 2011), will contribute further real-time insights into how specific regulatory sequence motifs and splicing protein factors influence intron dynamics and impinge on alternative splicing decisions.

See the Extended Discussion for more information.

EXPERIMENTAL PROCEDURES

Cells, Transfection, and RNA Analysis

All methods used for cell manipulations are described in detail in the Extended Experimental Procedures.

Spinning-Disk Confocal Microscopy and Image Analysis

Imaging was performed using a recently described microscopy setup (Boulant et al., 2011; Kural et al., 2012). For image analysis, we developed an application written in MATLAB (The MathWorks) to track single transcription sites in 3D and quantify their TFI over time by Gaussian fitting. The software was implemented as an interactive graphical user interface that allows for single time point analysis in a time lapse sequence as well as fully automated analysis of multiple time lapse sequences (batch processing mode), with parameterization of tracking and Gaussian fitting procedures and visualization of fitted data for quality assessment (Figure S3; see also Extended Experimental Procedures).

SUPPLEMENTAL INFORMATION

Supplemental Information includes an Extended Discussion, Extended Experimental Procedures, six figures, one table, and two movies and can be found with this article online at http://dx.doi.org/10.1016/j.celrep.2013.08.013.

ACKNOWLEDGMENTS

We gratefully acknowledge Eric Marino and members of the Kirchhausen laboratory for their help and support. We also thank M. Yoshida, Jens Lykke-Andersen, Niels Gehring, Edouard Bertrand, Jan Ellenberg, Michael Antoniou, and Juan Valcárcel for the gifts of spliceostatin A, MS2, BoxB, MS2-GFP, λN-GFP, β-globin plasmids, and IgM plasmids, respectively. We thank Marisa Cabrita and Sérgio Marinho for excellent technical help, and our colleagues José Braga, Noélia Custódio, Sandra Martins, and Sérgio de Almeida for insightful discussions. We also thank Stephen C. Harrison for a critical reading of the manuscript. This work was supported by a grant from Fundação para a Ciência e Tecnologia, Portugal (PTDC/SAU-GMG/118180/2010), and the Harvard Medical School-Portugal Program in Translational Research and Information. R.M.M. was supported by a grant from Fundação para a Ciência e Tecnologia, Portugal (SFRH/BPD/66611/2009), and received an EMBO Short Term Fellowship (ASTF272.00-2011). J.R. holds a Ciência 2008 position from the Portuguese Ministry of Science and Technology. E.M. was supported in part by grants from the National Institutes of Health (NIH U54 AI057159) and the New England Regional Center of Excellence in Biodefense and Emerging Infectious Diseases. T.K. was supported in part by NIH grant GM 075252.

Received: July 3, 2012
Revised: May 20, 2013
Accepted: August 7, 2013
Published: September 12, 2013

REFERENCES

Beyer, A.L., and Osheim, Y.N. (1988). Splice site selection, rate of splicing, and alternative splicing on nascent transcripts. Genes Dev. *2*, 754–765.

Bhatt, D.M., Pandya-Jones, A., Tong, A.J., Barozzi, I., Lissner, M.M., Natoli, G., Black, D.L., and Smale, S.T. (2012). Transcript dynamics of proinflammatory genes revealed by sequence analysis of subcellular RNA fractions. Cell *150*, 279–290.

Boulant, S., Kural, C., Zeeh, J.C., Ubelmann, F., and Kirchhausen, T. (2011). Actin dynamics counteract membrane tension during clathrin-mediated endocytosis. Nat. Cell Biol. *13*, 1124–1131.

Chubb, J.R., and Liverpool, T.B. (2010). Bursts and pulses: insights from single cell studies into transcriptional mechanisms. Curr. Opin. Genet. Dev. *20*, 478–484.

Cooper, T.A., Wan, L., and Dreyfuss, G. (2009). RNA and disease. Cell *136*, 777–793.

Corrionero, A., Miñana, B., and Valcárcel, J. (2011). Reduced fidelity of branch point recognition and alternative splicing induced by the anti-tumor drug spliceostatin A. Genes Dev. *25*, 445–459.

Custódio, N., Carmo-Fonseca, M., Geraghty, F., Pereira, H.S., Grosveld, F., and Antoniou, M. (1999). Inefficient processing impairs release of RNA from the site of transcription. EMBO J. *18*, 2855–2866.

Daigle, N., and Ellenberg, J. (2007). LambdaN-GFP: an RNA reporter system for live-cell imaging. Nat. Methods *4*, 633–636.

Danko, C.G., Hah, N., Luo, X., Martins, A.L., Core, L., Lis, J.T., Siepel, A., and Kraus, W.L. (2013). Signaling pathways differentially affect RNA polymerase II initiation, pausing, and elongation rate in cells. Mol. Cell *50*, 212–222.

Darzacq, X., Shav-Tal, Y., de Turris, V., Brody, Y., Shenoy, S.M., Phair, R.D., and Singer, R.H. (2007). In vivo dynamics of RNA polymerase II transcription. Nat. Struct. Mol. Biol. *14*, 796–806.

Das, R., Dufu, K., Romney, B., Feldt, M., Elenko, M., and Reed, R. (2006). Functional coupling of RNAP II transcription to spliceosome assembly. Genes Dev. *20*, 1100–1109.

de Almeida, S.F., García-Sacristán, A., Custódio, N., and Carmo-Fonseca, M. (2010). A link between nuclear RNA surveillance, the human exosome and RNA polymerase II transcriptional termination. Nucleic Acids Res. *38*, 8015–8026.

de la Mata, M., Alonso, C.R., Kadener, S., Fededa, J.P., Blaustein, M., Pelisch, F., Cramer, P., Bentley, D., and Kornblihtt, A.R. (2003). A slow RNA polymerase II affects alternative splicing in vivo. Mol. Cell *12*, 525–532.

Dye, M.J., and Proudfoot, N.J. (1999). Terminal exon definition occurs cotranscriptionally and promotes termination of RNA polymerase II. Mol. Cell *3*, 371–378.

Eperon, L.P., Graham, I.R., Griffiths, A.D., and Eperon, I.C. (1988). Effects of RNA secondary structure on alternative splicing of pre-mRNA: is folding limited to a region behind the transcribing RNA polymerase? Cell *54*, 393–401.

Franklin, N.C. (1985). Conservation of genome form but not sequence in the transcription antitermination determinants of bacteriophages lambda, phi 21 and P22. J. Mol. Biol. *181*, 75–84.

Grünwald, D., and Singer, R.H. (2010). In vivo imaging of labelled endogenous β-actin mRNA during nucleocytoplasmic transport. Nature *467*, 604–607.

Hocine, S., Raymond, P., Zenklusen, D., Chao, J.A., and Singer, R.H. (2013). Single-molecule analysis of gene expression using two-color RNA labeling in live yeast. Nat. Methods *10*, 119–121.

Hoskins, A.A., Friedman, L.J., Gallagher, S.S., Crawford, D.J., Anderson, E.G., Wombacher, R., Ramirez, N., Cornish, V.W., Gelles, J., and Moore, M.J. (2011). Ordered and dynamic assembly of single spliceosomes. Science *331*, 1289–1295.

Kaida, D., Motoyoshi, H., Tashiro, E., Nojima, T., Hagiwara, M., Ishigami, K., Watanabe, H., Kitahara, T., Yoshida, T., Nakajima, H., et al. (2007). Spliceostatin A targets SF3b and inhibits both splicing and nuclear retention of pre-mRNA. Nat. Chem. Biol. *3*, 576–583.

Kessler, O., Jiang, Y., and Chasin, L.A. (1993). Order of intron removal during splicing of endogenous adenine phosphoribosyltransferase and dihydrofolate reductase pre-mRNA. Mol. Cell. Biol. *13*, 6211–6222.

Kural, C., Tacheva-Grigorova, S.K., Boulant, S., Cocucci, E., Baust, T., Duarte, D., and Kirchhausen, T. (2012). Dynamics of intracellular clathrin/AP1- and clathrin/AP3-containing carriers. Cell Rep. *2*, 1111–1119.

Larson, D.R., Zenklusen, D., Wu, B., Chao, J.A., and Singer, R.H. (2011). Real-time observation of transcription initiation and elongation on an endogenous yeast gene. Science *332*, 475–478.

Lionnet, T., Czaplinski, K., Darzacq, X., Shav-Tal, Y., Wells, A.L., Chao, J.A., Park, H.Y., de Turris, V., Lopez-Jones, M., and Singer, R.H. (2011). A transgenic mouse for in vivo detection of endogenous labeled mRNA. Nat. Methods *8*, 165–170.

Lowary, P.T., and Uhlenbeck, O.C. (1987). An RNA mutation that increases the affinity of an RNA-protein interaction. Nucleic Acids Res. *15*, 10483–10493.

Maniatis, T., and Reed, R. (2002). An extensive network of coupling among gene expression machines. Nature *416*, 499–506.

Martins, S.B., Rino, J., Carvalho, T., Carvalho, C., Yoshida, M., Klose, J.M., de Almeida, S.F., and Carmo-Fonseca, M. (2011). Spliceosome assembly is coupled to RNA polymerase II dynamics at the 3′ end of human genes. Nat. Struct. Mol. Biol. *18*, 1115–1123.

Nilsen, T.W., and Graveley, B.R. (2010). Expansion of the eukaryotic proteome by alternative splicing. Nature *463*, 457–463.

Niwa, M., MacDonald, C.C., and Berget, S.M. (1992). Are vertebrate exons scanned during splice-site selection? Nature *360*, 277–280.

Nogues, G., Kadener, S., Cramer, P., Bentley, D., and Kornblihtt, A.R. (2002). Transcriptional activators differ in their abilities to control alternative splicing. J. Biol. Chem. *277*, 43110–43114.

Roybal, G.A., and Jurica, M.S. (2010). Spliceostatin A inhibits spliceosome assembly subsequent to prespliceosome formation. Nucleic Acids Res. *38*, 6664–6672.

Shav-Tal, Y., Darzacq, X., Shenoy, S.M., Fusco, D., Janicki, S.M., Spector, D.L., and Singer, R.H. (2004). Dynamics of single mRNPs in nuclei of living cells. Science *304*, 1797–1800.

Singh, J., and Padgett, R.A. (2009). Rates of in situ transcription and splicing in large human genes. Nat. Struct. Mol. Biol. *16*, 1128–1133.

Staley, J.P., and Guthrie, C. (1998). Mechanical devices of the spliceosome: motors, clocks, springs, and things. Cell *92*, 315–326.

Tsurushita, N., Avdalovic, N.M., and Korn, L.J. (1987). Regulation of differential processing of mouse immunoglobulin mu heavy-chain mRNA. Nucleic Acids Res. *15*, 4603–4615.

Valegård, K., Murray, J.B., Stockley, P.G., Stonehouse, N.J., and Liljas, L. (1994). Crystal structure of an RNA bacteriophage coat protein-operator complex. Nature *371*, 623–626.

Vargas, D.Y., Shah, K., Batish, M., Levandoski, M., Sinha, S., Marras, S.A., Schedl, P., and Tyagi, S. (2011). Single-molecule imaging of transcriptionally coupled and uncoupled splicing. Cell *147*, 1054–1065.

Watakabe, A., Inoue, K., Sakamoto, H., and Shimura, Y. (1989). A secondary structure at the 3′ splice site affects the in vitro splicing reaction of mouse immunoglobulin mu chain pre-mRNAs. Nucleic Acids Res. *17*, 8159–8169.

Watakabe, A., Tanaka, K., and Shimura, Y. (1993). The role of exon sequences in splice site selection. Genes Dev. *7*, 407–418.

Wetterberg, I., Zhao, J., Masich, S., Wieslander, L., and Skoglund, U. (2001). In situ transcription and splicing in the Balbiani ring 3 gene. EMBO J. *20*, 2564–2574.

Will, C.L., and Lührmann, R. (2011). Spliceosome structure and function. Cold Spring Harb. Perspect. Biol. *3*, 3.

Wu, B., Chao, J.A., and Singer, R.H. (2012). Fluorescence fluctuation spectroscopy enables quantitative imaging of single mRNAs in living cells. Biophys. J. *102*, 2936–2944.